NeuroImage 47 (2009) 42–49

Contents lists available at ScienceDirect

NeuroImage

journal homepage: www.elsevier.com/locate/ynimg

Technical Note

Advances in high-resolution imaging and computational unfolding of the human hippocampus

Arne D. Ekstrom [a,b], Adam J. Bazih [a], Nanthia A. Suthana [a], Ramsey Al-Hakim [a], Kenji Ogura [a], Michael Zeineh [c], Alison C. Burggren [a], Susan Y. Bookheimer [a,*]

[a] Center for Cognitive Neuroscience, Semel Institute, Department of Psychiatry and Biobehavioral Sciences, University of California, Los Angeles, CA, USA
[b] Center For Neuroscience, Department of Psychology, University of California, Davis, CA, USA
[c] Stanford Medical School, Palo Alto, CA, USA

ARTICLE INFO

Article history:
Received 27 September 2008
Revised 9 February 2009
Accepted 4 March 2009
Available online 19 March 2009

Keywords:
Hippocampus
MRI
fMRI
High-resolution imaging

ABSTRACT

The hippocampus is often a difficult structure to visualize with magnetic resonance imaging (MRI) and functional MRI (fMRI) due to its convoluted nature and susceptibility to signal dropout. Improving our ability to pinpoint changes in neural activity using fMRI in this structure remains an important challenge. Current fMRI/MRI methods typically do not permit visualization of the hippocampus and surrounding cortex at a resolution less than 1 mm. We present here improvements to our previous methods for obtaining structural MR images of the hippocampus, which provided an in-plane resolution of 0.4 mm^2 mm and two-dimensional "flat" maps of the hippocampus with an interpolated isotropic resolution of 0.4 mm^3 (Engel, S.A., Glover, G.H., and Wandell, B.A., (1997). Retinotopic organization in human visual cortex and the spatial precision of functional MRI. Cereb. Cortex 7, 181–192.; Zeineh, M.M., Engel, S.A., and Bookheimer, S.Y., (2000). Application of cortical unfolding techniques to functional MRI of the human hippocampal region. NeuroImage 11, 668–683.). We present changes to existing structural imaging sequences that now augment the resolution of previous scans, permitting visualization of the anterior portion of CA1, parts of the dentate gyrus, and CA23. These imaging improvements are of relevance generally to the field of imaging because they permit higher overall resolution imaging of the hippocampus than previously possible (at 3 T). We also introduce a novel application of a computational interpolation method that improves our ability to capture the convoluted three-dimensional shape of the hippocampus. Furthermore, we have developed a quantitative method for obtaining group activation patterns based on producing averaged flat maps using vector field warping techniques, allowing localization of activations to specific hippocampal subregions across groups of subjects. Together, these methods provide a means to improve imaging of neural activity in the human hippocampus and surrounding cortex during cognitive tasks.

Introduction

The hippocampal area, including subregions of the hippocampus such as the dentate gyrus, the cornus amonis fields (CA1–3), and the subiculum, together with surrounding cortices (i.e., entorhinal, perirhinal, and parahippocampal cortices), plays critical and selective roles in learning and memory. Studies employing electrophysiological recordings in the rodent have elucidated separate roles in memory encoding and retrieval for the dentate gyrus (Leutgeb et al., 2007), CA3 (Lee et al., 2004), CA1 (Lee et al., 2004; Wilson and McNaughton, 1993), and subiculum (Sharp, 2006; Sharp and Green, 1994). Primate and rodent electrophysiological studies have also revealed distinct roles for the surrounding entorhinal, perirhinal, and parahippocampal in memory (Aggleton and Brown, 2006; Brown and Aggleton, 2001; Ekstrom et al., 2003; Fyhn et al., 2004). Despite this extensive body of knowledge from single cell recordings, little progress has been made in gaining similar knowledge about the roles of hippocampal subregions in human memory. This is largely because current non-invasive imaging methods (i.e., fMRI) typically lack the spatial resolution to image subregions of the human hippocampal area.

Recent advances in imaging of the hippocampus, though, have made some progress in visualizing subregions of the hippocampus such as CA1, subiculum, CA23/dentate gyrus, and surrounding cortex. These methods have approached the challenge of imaging the hippocampus using two distinct techniques. The first involves using high-resolution anatomical T1-weighted MP-RAGE sequences (Bakker et al., 2008; Kirwan et al., 2007; Miller et al., 2005) to produce isotropic voxels of 0.75 mm. A second line of investigation employs anatomical T2-weighted images with high in-plane resolution (0.4 mm in the oblique coronal plane) and 3 mm in the longitudinal plane (Burggren et al., 2008; Ekstrom et al., 2008; Eldridge et al., 2005; Zeineh et al., 2000; Zeineh et al., 2001; Zeineh et al., 2003). The hippocampus is then

* Corresponding author. Center for Cognitive Neuroscience, Semel Institute, UCLA, 760 Westwood Plaza, Los Angeles, CA 90095-7039, USA.
E-mail address: sbook@ucla.edu (S.Y. Bookheimer).

1053-8119/$ – see front matter © 2009 Elsevier Inc. All rights reserved.
doi:10.1016/j.neuroimage.2009.03.017

manually segmented, interpolated, and computationally unfolded to a final voxel size of 0.4 mm. In both methods, group maps are produced based on "warping" individual hippocampi into a common plane, thus basing group maps on individual hippocampi rather than fitting to a template (Miller et al., 2005; Stark and Okado, 2003; Thompson et al., 2000). Both methods then rely on high-resolution blood oxygen level-dependent (BOLD) sequences (1.5 mm isotropic for the first vs. 1.6 mm × 1.6 × 3 mm for the second) to image and localize functional activity. Other methods using high-field structural imaging offer promise for significantly greater resolution but are currently limited to post-mortem brains (Augustinack et al., 2005).

One limitation of current high-resolution anatomical imaging methods is that they have not been able to discriminate anterior CA fields from dentate gyrus or dentate gyrus from CA23 in the posterior plane due to insufficient MR resolution. The methods that we present here expand on our previous methods (e.g., Zeineh et al. 2000, 2001, 2003) using high-resolution T2 weighted anatomical images prescribed to the hippocampal area coupled with high-resolution echo-planar imaging (EPI). We present several new imaging sequences that simultaneously improve our resolution in the longitudinal plane from 3 mm to 1 mm and furthermore enhance our ability to visualize subregions of the hippocampus. We also present a novel application of a computational interpolation method that improves our ability to detect changes along the longitudinal axis of the hippocampus. The software we present is now compatible with other functional imaging software packages such as SPM (Friston et al., 1995), FSL (Woolrich et al., 2001), and AFNI (Cox, 1996) and are available for download from our website. Together, the methods we present here improve over earlier techniques in allowing visualization of changes in hippocampal activity.

Materials and methods

Data acquisition

A series of nine scan sets were collected with the purpose of decreasing slice thickness and increasing the number of oblique slices through the hippocampus. These sequences were run with a total of 6 different subjects each (3 male, 3 female) with a mean age of 30 (range: 22–52), each of whom provided informed consent. Structural MRI scans were collected on a Siemens Allegra 3 T scanner (Siemens AG) with an eight-channel head coil at the Ahmanson-Lovelace Brain Mapping Center (Los Angeles, CA). Our earlier hippocampal high-resolution scans achieved voxel sizes of 0.4 × 0.4 × 3.0 mm with approximately 19 slices. To increase the number of hippocampal slices to 35–40, while reducing slice thickness to roughly 1 mm, new sequence changes were necessary (see Table 1). By increasing the number of scan averages (NEX) to three, combined with base resolution changes, it was possible to enhance image clarity while keeping scan times at a minimum. The adverse effects of decreasing base resolution were compensated with adjustments to the field of view (FoV), flip angle, and echo times (TE). These parameters, combined with three averages, achieved a more desirable balance of signal-to-noise ratio (SNR) and improved overall resolution.

Table 1

Parameter	HHR structural (original)	HHR structural[a] (HR_108)	HHR structural[a] (HR_109)
TR (ms)	5200	3640	10 000
TE (ms)	105	114	102
Number of slices	19	40	36
Slice thickness (mm)	3	1.20	1.00
Distance factor (%)	0	0	0
Phase Encoding Direction	F ≫ H	F ≫ H	F ≫ H
FoV RO	200	195	195
FoV phase	200	100	99.1
Concatenations	1	1	1
Fat suppression	None	None	None
Measurements	1	1	1
Voxel size	0.4 × 0.4 × 3 mm	0.5 × 0.5 × 1.2 mm^3	0.4 × 0.4 × 1.0 mm^3
Partial Fourier	Off	Off	Off
BW	195	195	195
Echo spacing (ms)	10.5	10.5	10.5
Time (min)	6:10	9:37	6:21

[a] Relative SNR = 1.00 tse.

Segmentation and demarcation of subregional boundaries

We first manually segment hippocampal gray matter by outlining white matter and CSF along hippocampus proper and extending through fusiform cortex (Fig. 1). This is done using mrGray software (Teo et al., 1997), which permits the user to create distinct masks or "label-maps" separately for CSF and white matter (download: http://white.stanford.edu/software/). Masks are based on changes in intensity values visible on the MR images.

Automated interpolation

A sequential algorithm was developed in Matlab (by R.A-H.) to interpolate segmentation masks and hippocampal images prior to flattening in order to produce higher resolution maps; this served as a replacement for the manual interpolation methods used previously (Zeineh et al., 2001). We use the term "sequential" here to indicate that the algorithm is actually a series of multiple steps, consisting of the following: interpolation, anisotropic curvature smoothing, thresholding, and 3-D rendering. The data collected from the scanner varied in slice thickness (mm/slice) depending on the case. Thus, the goal of the sequential algorithm was to take any segmented image series and interpolate them only along the *z*-axis (i.e., between the images) to produce the desired, enhanced slice thickness (download, visit: http://airto.hosted.ats.ucla.edu/Hippocampus/Segmentation.html).

Since the manually-created label-map only isolated the white matter and CSF, the first step of the algorithm was to automatically label the gray matter by exclusion. To accomplish this, the background was labeled automatically by classifying as background the value of the pixel at the top-left corner of each image. All voxels not identified as background, CSF or white matter were assigned to gray matter. The white and gray matter pixels were placed into separate volumes (a series of label-map images is referred to here as a volume) with an intensity range of 0–255. The background was labeled with intensity zero and the gray and white matter were labeled in their separate volumes as 128. These volumes were then automatically interpolated along the *z*-axis using a linear interpolation method to create the increased desired *z*-axis resolution as specified by the user (0.4 mm). Preliminary tests were made of more complex methods of interpolation such as cubic and spline, but these caused significantly enhanced computation time with no considerable improvement in interpolation quality.

The separate gray and white volumes created from interpolation were then smoothed using an anisotropic curvature "smoother" developed by Oliver et al. (1997). This smoothing algorithm has the effect of dampening high curvature areas of the surfaces in the volume, but does not smooth across boundaries with white matter or CSF. Thus, the result is a smooth volume with preserved sharp intensity edges defining the boundaries between structures. This smoothing method was selected purposely to prevent "bridges" or "holes" (discontinuities) from developing in the surface of the hippocampus structure. A default threshold was applied separately to each volume such that only pixels with intensity greater than 128 were labeled as white or gray matter.

The results from thresholding each volume separately were finally combined to produce one volume with gray, CSF, and white matter labeled. This created an initial label-map of the gray, CSF, and white matter of the hippocampus with the desired slice thickness (Fig. 1).

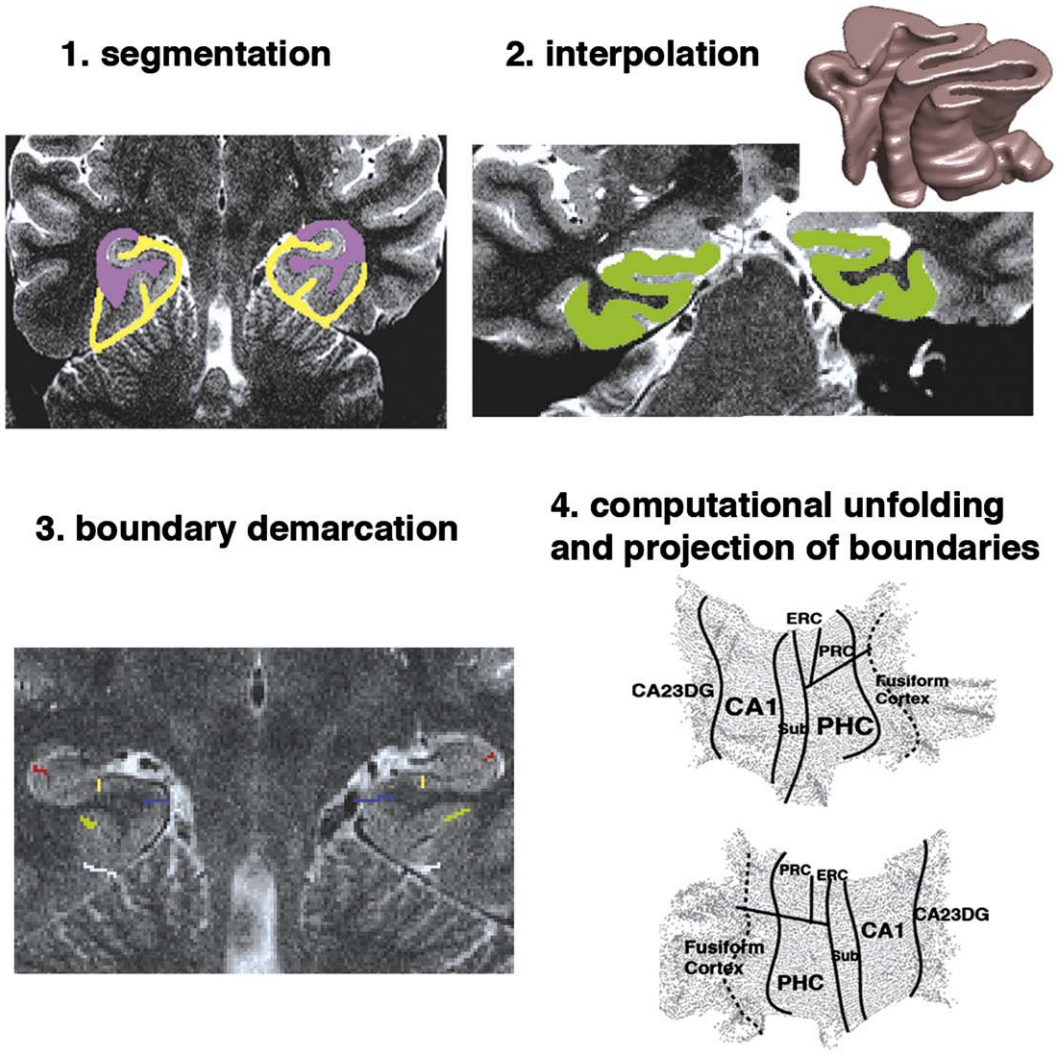

Fig. 1. Methods for producing hippocampal flat maps: Segmentation (purple colors show segmented white matter, yellow colors show segmented CSF), interpolation (green shows interpolated gray matter derived from segmentation), boundary demarcation (colors show boundaries subsequently labeled in Fig. 2; see Fig. 2 for details), and computational unfolding and boundary projection.

For quality control, a three-dimensional surface model rendering of the gray matter was generated so as to allow the user to visually inspect for the aforementioned bridges and holes (which, if present, could be manually corrected on the segmentation).

Computational unfolding and boundary demarcation

The three-dimensional (3-D) gray matter strip is then computationally flattened into two-dimensions (2-D) using mrUnfold software (Engel et al., 1997). Each layer of gray matter is computationally unfolded separately onto a flat image. Once we have flattened all the layers of gray matter that have been defined through interpolation, we obtain a 3-D to 2-D transformation that can be used to map subregional boundaries and functional activations into flat space (download: http://sourceforge.net/projects/mtl-unfolding/). In the boundary demarcation step (Fig. 1), we use landmarks on the 3-D hippocampal scan to define anatomical boundaries of CA1-CA23DG, CA1-Subiculum (Sub), Sub-entorhinal cortex (ERC), ERC-perirhinal cortex (PRC), subiculum-parahippocampal (PHC) cortex, and PHC-Fusiform Cortex (e.g., the collateral sulcus) (Amaral and Insausti, 1990; Duvernoy, 1998). We also demarcate the beginning of hippocampal head (Anterior CADG) and the ERC-PRC-PHC boundary. In the boundary projection step (Fig. 1), these boundaries are then projected into a computationally flattened 2-D image of the hippocampus, thus outlining the anatomical locations defined by these boundaries in 3-D space. Boundaries are defined in flat space by computing the best-fit fourth order polynomial. Comparable examples of computational hippocampal unfolding methods are also presented elsewhere (Burggren et al., 2008; Ekstrom et al., 2008; Zeineh et al., 2001, 2003). Validation and precision of the method can be found in Zeineh et al. 2001. Intra-subject reliability assessments can be found in Burggren et al., 2008. Briefly, one rater repeated the entire analysis on six subjects and calculated reliability for measurements of cortical thickness and volume. We used the intra-class correlation coefficient (ICC) to evaluate intra-rater reliability and additionally reported the standard error of the mean (Burggren et al. 2008). ICC values ranged from 0.967 to 0.996 and SEM values from 0.045 to 0.047.

Calculating cortical thickness

From these flat maps, we could then produce cortical thickness measurements. We did this initially in 3-D space as follows: for each gray matter voxel in each layer of the manifold we computed the distance to the closest non-gray matter voxel (white matter or CSF). Voxels from three-dimensional space were then projected into two-dimensional space; if several voxels projected from three-dimensional space to the same voxel in two-dimensional space, the maximum thickness of the voxels (rather than the mean as used for activations)

was taken. This ensured that thickness values represented the largest values across the gray matter strip. See Burggren et al., 2008 for more details on calculating cortical thickness.

Trouble-shooting unfolding

Occasionally, segmentation and automated interpolation led to the previously mentioned discontinuities in flat maps despite our attempts to deal with this during automated interpolation and in mrGray (which contains an option to detect these so called "handles"). These more subtle discontinuities could be detected by abnormal boundary projections in flat space. As a means of further checking results of flat mapping, we back-projected boundary demarcations onto three-dimensional MRIs to verify accurate projection (Fig. 2). Discontinuities then could be detected however by either a failure of the boundaries to project, leading to the best-fit lines to intersect other best-fit lines or inaccurate back-projection of regions of the hippocampus. When either of these cases arose, hippocampi were re-segmented and re-interpolated to remove any discontinuities that may have not been detected during interpolation (in practice, these occurred rarely). In Figs. 2e, f, we show that regions back-project from flat space accurately in this test case.

Functional imaging

Subjects performed three runs in a blocked-design, virtual navigation experiment as they were scanned with high-resolution EPI sequences (TR = 2 s,TE = 39 ms, slices = 19, voxel size = $1.6 \times 1.6 \times 3$ mm^3). The experiment was programmed in python using the virtual navigation engine "yellowcab" (Caplan et al., 2003). The task was administered by projecting it from a Macintosh lap-top display into MR-compatible goggles in the scanner room. Subjects freely navigated using an MR-compatible joystick. In each navigation block, subjects explored a virtual environment by searching for passengers and delivering them to stores for 120 s, and then subjects followed arrows on the screen with the joystick for 25 s; this sequence repeated 8 times over the three runs. Subjects encountered one passenger per trial, which they were instructed to bring to a specific store. There were eight different destination stores and eight different passengers, with four separate deliveries to each destination interspersed over the course of the experiment. Our control task was based on previous findings suggesting that low-level perceptual tasks, such as determining the direction of an arrow, provide minimal hippocampal activation compared to other conditions (Stark and Squire, 2001). A matched-bandwidth sequence (TR = 5 s, TE = 66 ms, voxel size = $1.6 \times 1.6 \times 3$ mm) permitted registration of EPI sequences to the hippocampal structural scan (TR = 5.2 s, TE = 105 ms, voxel size: $0.4 \times 0.4 \times 3$ mm).

Significant regions of functional activations were evaluated using FSL FEAT, e.g., http://www.fmrib.ox.ac.uk/fsl/feat5/ (Woolrich et al., 2001). We applied motion correction, high-pass filtering (100 s), and spatial smoothing (5 mm). Activations were modeled using a blocked-design analysis using the GLM (Beckmann et al., 2003) with equivalent amounts of navigation and control tasks (25 s of navigation compared to 25 s of the control). Subsequent navigational epochs were factored out as a 3rd explained variable to be consistent with previous results (Aguirre et al., 1996). Functional activations were projected to flat space as follows. A computational algorithm was used to project the activation pixels from 3-

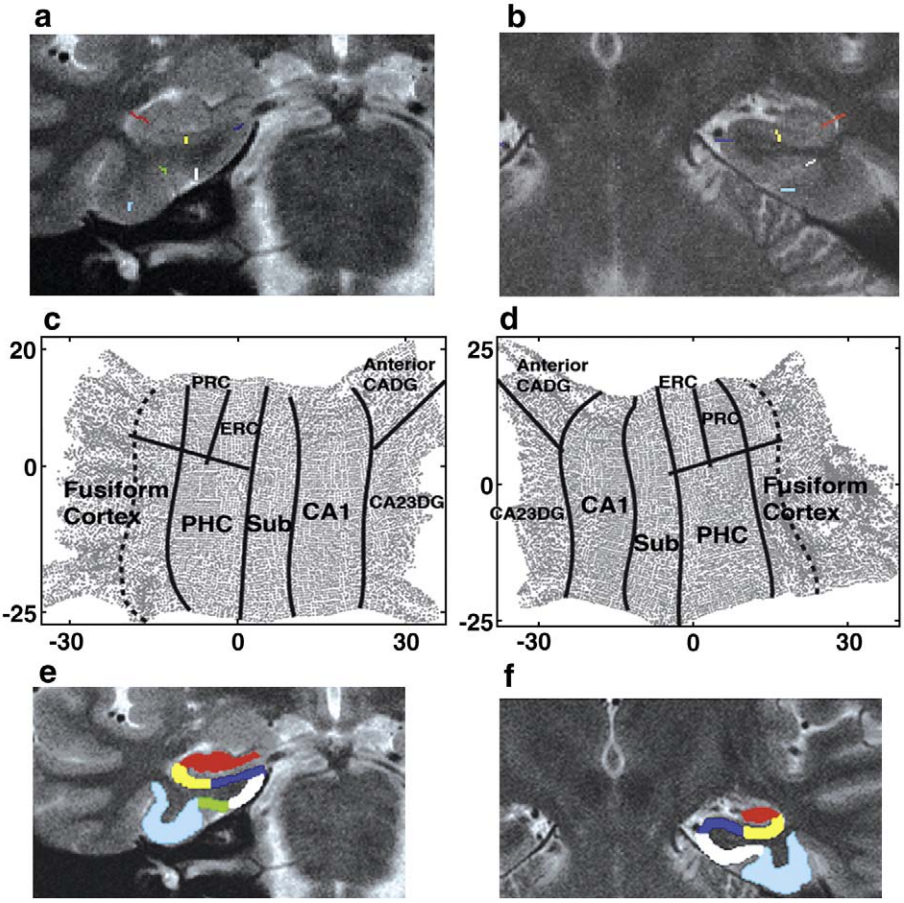

Fig. 2. Right and left (a) anterior and (b) medial hippocampus on $0.4 \times 0.4 \times 3$ mm anatomical T2 weighted image with demarcated hippocampal boundaries. (c, d) Right and left hippocampal flat maps produced from these same images. (e, f) Back-projection of subfields derived from flatmaps on to 3-D anatomical images. Red area, CA2/CA3/dentate gyrus (CA23DG); yellow area, CA1; dark blue area, subiculum (Sub); green area, PRC; white area, ERC; light blue area, fusiform cortex.

D to 2-D using the exact transformation that was used to project pixels from the 3-D anatomical images to the 2-D flat map. Because several voxels may have projected to only one pixel in flat space, we took the mean over multiple voxels in 3D space and projected this value into 2-D space. Thus, each activation pixel in flat space represents the mean of the slope of the fit between behavioral data and the fMRI time course data (i.e., β-weight) obtained in 3-D space. β-weights are then transformed into *z* values later during group mapping (see below).

Hippocampal activation group maps

Group activation maps were produced by averaging the subregional boundaries of each subject and then transforming each subject's flat map to this template (Thompson et al., 2000). Individual subject boundaries were resampled to 100 uniformly spaced points and vector averaged across subjects, producing an average anatomic template. Transformations for each subject to this template were derived as follows: each of the 100 points on each boundary was displaced to match the template, and an elastic body deformation field was computed for the rest of the points to produce a field that minimizes changes in area. For calculating BOLD activations across subjects, the degree of fit between each individual subject's behavior and the BOLD signal (e.g., beta values) were compared across subjects for each voxel using a mixed-effects *t*-test. Significance thresholds for activations were set at $p<0.05$ and $t>2.4$.

Results

Compared to the $0.4\times0.4\times3$ mm images (i.e., our original sequence), the $0.5\times0.5\times1.2$ mm and $0.4\times0.4\times1$ mm images provided three times (or nearly three times) as many slices and, at

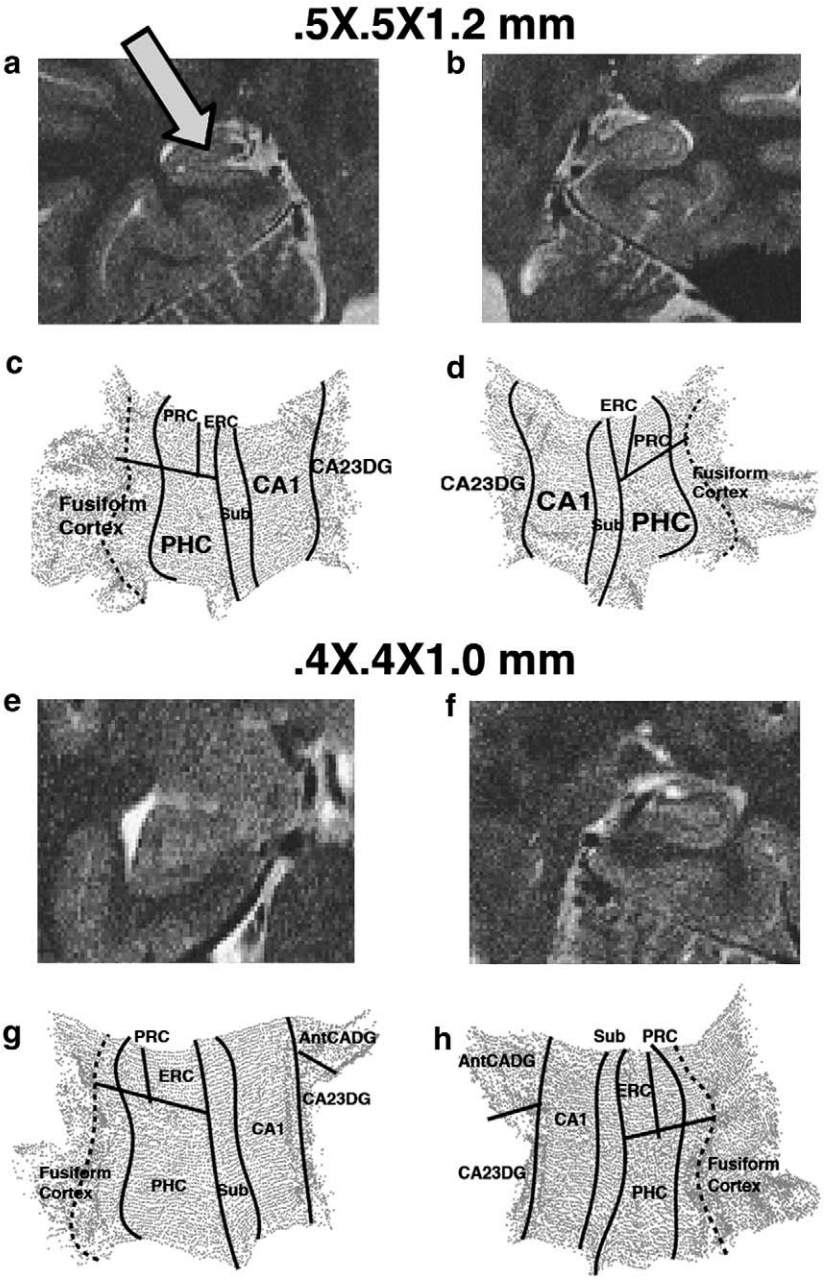

Fig. 3. (a) Slice from $0.5\times0.5\times1.2$ mm sequences (see Table 1). CA3 and dentate gyrus are visible on this slice, CA3 is pointed to with arrow. b) Another slice from the same sequences in (a) taken from the anterior portion of the hippocampus. CA3-DG and CA1 can be demarcated on this slice. (c, d) Right and left hippocampal flat maps derived from the image sequence from in (a and b). Anterior CA1 is separated from CA3-DG, which was not possible in earlier imaging sequences. (e, f) Two slices from $0.4\times0.4\times1$ mm sequence. (g, h) Hippocampal flat maps produced from the $0.4\times0.4\times1$ mm sequence. Due to a slightly lower SNR in these images, the same anatomical designations possible in a,b,c,d could not be made here.

least for the 0.5×0.5×1.2 mm images, comparable (if not better, in some cases) in-plane resolution. On the 0.5×0.5×1.2 images, CA1 could be reliably identified on anterior images, demarcated, and projected into flat space (Fig. 3b). Also in the 0.5×0.5×1.2 images, on some slices, CA23 and dentate gyrus could be reliably distinguished (Figs. 3a, b), although they were not sufficiently present across slices to be projected into flat space. While we obtained sufficient resolution in the 0.4×0.4×1 mm images (Figs. 3e–h) to visualize the same structures we typically demarcate in our 0.4×0.4×3 mm scans, we could not distinguish the same details as on the 0.5×0.5×1.2 mm scan, which was likely due to decreased SNR (SNR = 1.09 for the 0.5×0.5×1.2 mm scan; SNR = 1.00 for the 0.4×0.4×1 mm scan) obtained during the higher resolution images which was compensated for by reducing the resolution slightly. We note that although flat maps are of the same resolution as flat maps shown in Fig. 1 (obtained at 0.4×0.4×3 mm resolution and interpolated 7 times to 0.4 mm^3), these images are interpolated by a factor of 2 rather than 7. Thus, these flat maps contain approximately 3 times more anatomical information in the *Z* plane than in the 0.4×0.4×3 mm sequences.

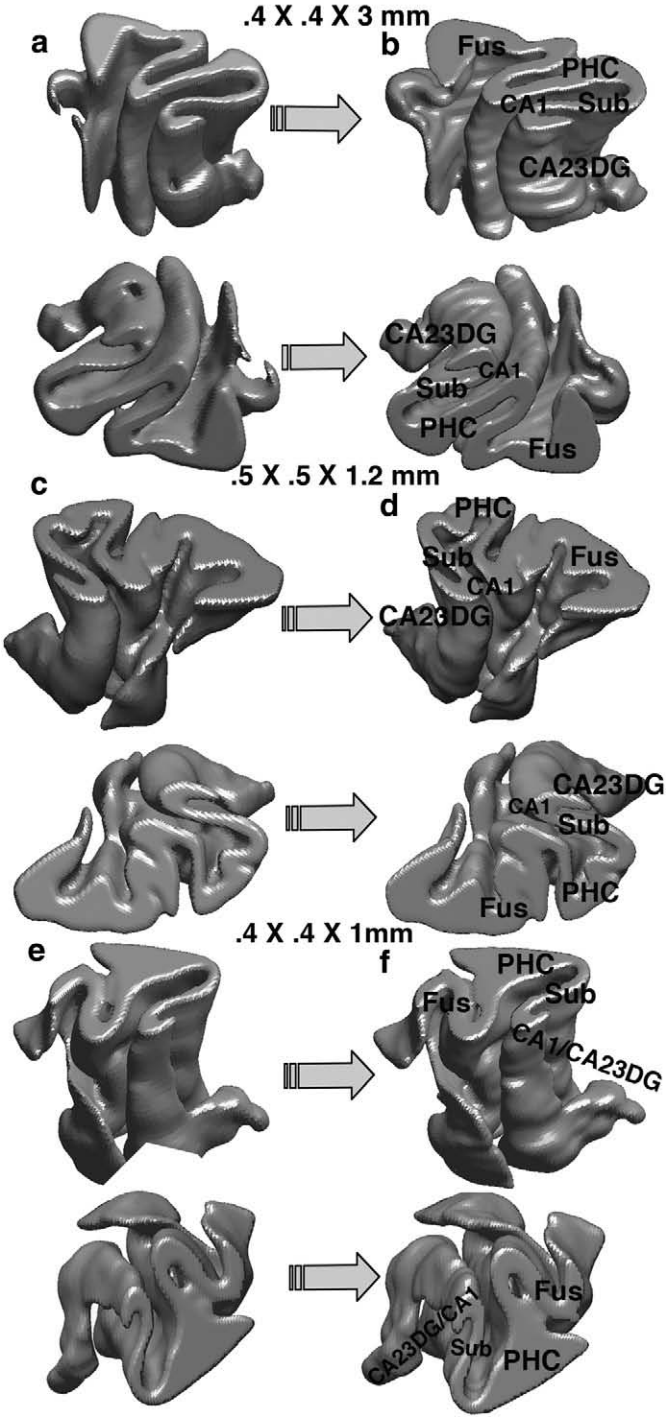

Fig. 4. (a, b) 3-D interpolation of a segmented hippocampus based on the 0.4×0.4×3 mm sequence. Holes and bridges, or discontinuities, are visible in the original images (shown in a) but much less so in the interpolated images (shown in b). Top and bottom row show different perspectives on same hippocampus to better illustrate areas of discontinuities. (c, d) Interpolation of 0.5×0.5×1.2 mm sequences and (e, f) 0.4×0.4×1 mm sequences. In both cases (e.g., c–f), the original anatomy is better preserved in the lower slice thickness sequences following interpolation than in the higher slice thickness sequences (shown in a, b).

Automated interpolation of hippocampal images revealed the occasional presence of discontinuities in manual segmentation, noted as a concern in the methods. These arise due to the presence of jumps between slices in the *Z* plane (Figs. 4a, c, e) and were smoothed out during interpolation while still preserving original anatomy (Figs. 4b, d, f). As can be seen in Figs. 4d, f, which are based on the 0.5×0.5×1.2 mm and 0.4×0.4×1 mm images, the interpolation, while still occasionally catching some discontinuities, makes fewer changes to the original anatomy in the ultra-high-resolution sequences compared to the higher slice thickness series (shown in Figs. 4a, b). This suggests, not surprisingly, that images obtained at lower slice thickness are advantageous anatomically because they capture more (approximately three times more, in this case) of the original structure of the hippocampus.

Individual flat maps were warped into group maps based on methods described previously (see Materials and methods; Figs. 5a, b). In the example shown, we plot the clusters of activations across a group of nine subjects (5 male, 4 female, mean age 25, range 20–31, all provided informed consent) who performed a navigation task. Subjects showed activations in the parahippocampal cortex and CA23DG and deactivations in hippocampus proper (e.g., CA1, CA23DG), consistent with previous results (Aguirre et al., 1996; Shipman and Astur, 2008).

Discussion

A critical challenge in neuroimaging is improving our detection of task-related, neural activity changes in subcortical structures and substructures in human brain. The hippocampus, a structure central to learning and memory, has proven difficult to image. Our prior work improved the resolution of functional and structural images of the hippocampus and surrounding cortex (Zeineh et al., 2001, 2003) and enhanced our ability to visualize activations in the hippocampus in groups of subjects. We present here modifications to these existing hippocampal anatomical imaging sequences that offer greater in-plane resolution of the hippocampus (Zeineh et al., 2000) compared to other methods using MP-RAGE sequences (Miller et al., 2005). This in-plane resolution confers a benefit of improved localization of cognitive task-dependent changes in the BOLD signal to specific spatial domains of the extended hippocampal formation. The modified sequences we present improve resolution in the longitudinal plane from 3 mm to 1 mm. While subfields can be most accurately identified in the coronal plane (medial–lateral plane), increased resolution in the anterior–posterior plane is also of importance to hippocampal function because of differences in inputs and processing in anterior compared to posterior hippocampus (Moser and Moser, 1998). Decreased slice thickness is also advantageous for improving accuracy in cortical thickness measurements, which can reveal subfield-specific atrophy that may underlie neurocognitive diseases such as Alzheimer's disease (Burggren et al., 2008; Han et al., 2006) and medial temporal lobe epilepsy (Mathern et al., 1996).

Following imaging with high-resolution anatomical and functional sequences, we next show that two-dimensional flat maps of the

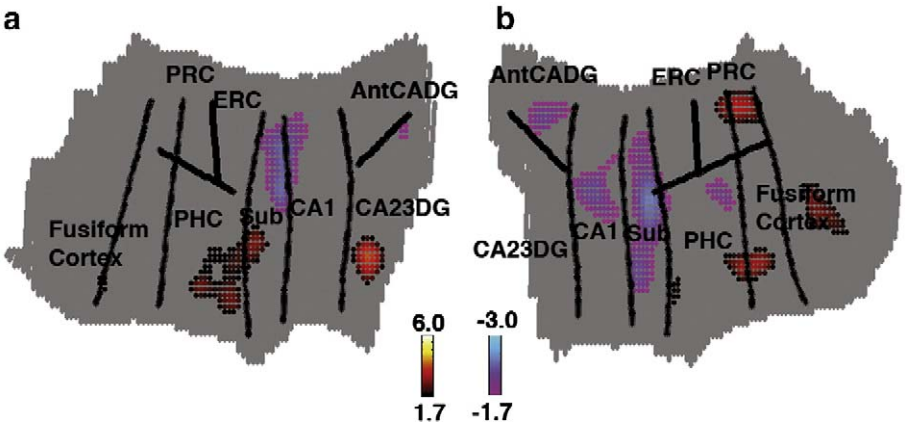

Fig. 5. Right and left group hippocampal flat map from nine subjects during virtual navigation. Positive (red) and negative (blue) activation clusters are clearly visible.

hippocampus can then be obtained from these imaging sequences. Flat maps are advantageous for several reasons. The structure of hippocampal subregions, as well activations along the long axis of the hippocampus, can be visualized in a single image of the hippocampus (see also Ekstrom et al., 2008). This permits visualization of patterns across the complex as a whole that are not easily discernable in slices. The organization of subregions in the HC is such that most extend along the long axis from the anterior to the posterior extent, but each area may comprise only a few voxels in-plane. In a study by Zeineh et al. (2003) for instance, the anterior/posterior dissociation between encoding and retrieval was easily discerned on the flat map. Similarly, the restriction of HC area activation to extrahippocampal structures (parahippocampal gyrus and fusiform gyrus) during the response of the hippocampus to novel stimuli was easily apparent on flat maps while this organization was difficult to discern in single slices (Zeineh et al., 2000). In our case, activations during virtual navigation that span part of the posterior parahippocampal cortex and negative activations in the medial hippocampus are clearly visible on a single image (Fig. 5), consistent with previous literature (Aguirre et al., 1996; Shipman and Astur, 2008).

Flat maps also allow greater resolution than can be obtained with our original anatomical images. Specifically, flat maps are interpolated down to a final isotropic voxel resolution of 0.4^3. These high-resolution maps can then be used to clearly visualize (interpolated) functional activations (Zeineh et al., 2003), localize electrodes in subfields of the hippocampus (Ekstrom et al., 2008), and provide enhanced information about the structural integrity of the hippocampus using measures such as cortical thickness (Burggren et al., 2008).

Finally, and perhaps most importantly, our present use of flat maps allows the warping of individual hippocampi into a common flat image, allowing group analyses within the hippocampus proper. This type of analysis has several advantages over the more common approach of registering individual hippocampi to a templates based on different brains such as the MNI or Talaraich template. The group anatomical maps obtained with our methods represent the actual anatomy of the group, which is particularly important with patient populations where hippocampal subfields may be degraded and thus be greatly out of register with a template based on normals (Thompson et al., 2000). Second, matching to templates is based on alignment of sulci and gyri of the entire brain, which in many cases will leave the hippocampi of individual subjects poorly aligned (Miller et al., 2005). Thus, because flat maps allow visualization of the hippocampus in an entire image, are of higher resolution, and can be used to produce group maps, flat mapping is advantageous to conventional imaging.

Some possible limitations to working with hippocampal flat maps warrant discussion. One issue, discussed previously in Hyde et al. (2001), is that scans resulting in isotropic voxels (e.g., the same size in three dimensions) may have advantages over non-isotropic scans, an issue of particular importance in BOLD imaging. While our interpolated flat maps are isotropic ($0.4\times0.4\times0.4$), our hippocampal anatomical and BOLD sequences are of high-resolution in-plane but are non-isotropic (1 to 3 mm in the longitudinal plane). We see no reason to believe, though, that significant amounts of information are lost when using non-isotropic voxels while much information is to be gained in a structure such as the hippocampus. In particular, our use of non-isotropic voxels in our scans permits higher in-plane resolution than is used in MR-RAGE sequences (0.4 vs. 0.75 mm), which is critical for accurately viewing and demarcating hippocampal subregions. Because variation in the HC architecture is minimal through plane and maximal within plane, it makes sense to maximize the in-plane resolution even at the cost of through plane resolution. Currently, SNR limitations limit our ability to improve from 1 mm to 0.4 mm in the longitudinal plane. We note that because of the linear relationship between SNR and magnet strength, higher Tesla magnets (e.g., 7 T) may offer one means of improving our overall voxel resolution and will be a focus of our future work.

A second concern may be related to the method or criteria we employed for demarcation of hippocampal subregions. Because MR technology cannot currently render *in vivo* brains at a comparable resolution to that at which post-mortem brains may be viewed at, we cannot definitively localize different cell layers and cell types and therefore cannot say with confidence exactly where one subregion begins and another ends. To attempt to deal with this particular issue, we employ the Duvernoy and Amaral and Insausti atlases, which are based on histological images of the hippocampus, so as to identify subregional boundaries. We look for changes in hippocampal shape and signal intensity on the MR image and then match to the same areas on histological images in the atlases. We have shown significant intra-rater reliability in the locations of subregions unfolded (Burggren et al., 2008). Future efforts based on probabilistic atlases and on patient population of post-mortem hippocampi will ultimately be necessary to determine how reliable the boundary demarcations are with respect to the underlying cellular anatomy.

A final concern regarding functional activations is how clusters of activations map for 3-D to 2-D. One potential concern here might be that clusters spreading through the medial–lateral axis of the hippocampus (e.g., from CA3 to subiculum) appear as multiple clusters due to the flat mapping. We deal with this issue by producing beta-weight values in FSL for all voxels, mapping to 2D, and then producing the thresholded and cluster-smoothed 2-D hippocampal map for the group. Because thresholding is done at the group level, clusters on individual subjects that cross hippocampal boundaries will not be maintained. Another potential issue with viewing activations in flat space is that not all voxels present in 3-D space will be present in

2-D space. As we note in the Materials and methods, activations in flat space were obtained by averaging voxels that project from 3-D (in cases where more than one voxel projects from 3-D space to 2-D space). Other investigators have attempted warping ("inflating") to alternative spaces such as spherical spaces (Fischl et al., 1999), which in principle would deal with the issue of voxel reduction in 2-D space. However, given the interdigitations of the CA fields and the dentate gyrus, this would potentially result in further distortions than flat space. Instead, future methodologic work may include 3-D spaces that involve less distortion. In particular, refolding our hippocampi (Zeineh et al., 2003) could produce a 3-D template to which we can ultimately directly warp our hippocampi.

We present here a methodology for imaging the hippocampus at high-resolution. Our method is an improvement on earlier methods presented by our lab, demonstrating that the hippocampus can be imaged at high-resolution ($0.4\times0.4\times1$–3 mm), computationally unfolded, and then combined with other hippocampal flat maps to produce group activations maps. These maps provide information about hippocampal subfields, information that cannot currently be obtained with conventional imaging techniques. Furthermore, the improvements to our methods that we present expand the resolution of our original high-resolution anatomical sequences from 3 mm to 1 mm, thus allowing clearer visualization of subregions such as CA3 and DG and CA1 from CA3-DG. Our sequences also provide clearer visualization of changes in hippocampal shape in the longitudinal plane. We also present an automated computational interpolation method that improves our ability to detect changes in the shape of the hippocampus along the longitudinal axis. Finally, we present improvements in our ability to detect functional changes in subjects' hippocampi at the individual and group level by introducing software that is compatible with functional activation software such as FSL, SPM, and AFNI. The group maps produced using this method allow clear visualization of clusters of activation in subfields of the hippocampus across a group of subjects. Together, these methods enhance our ability to detect subregion specific changes in BOLD activity in the hippocampus during behavior.

Acknowledgments

We thank Paul Thompson and Mark Cohen for contributing the computer code and technical guidance on the results in this manuscript. We thank John Melanokas for generous sharing of computer code central to the interpolation software. We thank Saba Movishari for technical assistance. We also thank NINDS F32 NS50067 for financial support to AE. For generous support the authors thank the Brain Mapping Medical Research Organization, Brain Mapping Support Foundation, Pierson-Lovelace Foundation, The Ahmanson Foundation, William M. and Linda R. Dietel Philanthropic Fund at the Northern Piedmont Community Foundation, Tamkin Foundation, Jennifer Jones-Simon Foundation, Capital Group Companies Charitable Foundation, Robson Family and Northstar Fund.

References

Aggleton, J.P., Brown, M.W., 2006. Interleaving brain systems for episodic and recognition memory. Trends Cogn. Sci. 10, 455–463.
Aguirre, G.K., Detre, J.A., Alsop, D.C., D'Esposito, M., 1996. The parahippocampus subserves topographical learning in man. Cereb. Cortex 6, 823–829.
Amaral, D.G., Insausti, R., 1990. The hippocampal formation. In: Paxinos, G. (Ed.), The Human Nervous System. Academic Press, San Diego, pp. 711–755.
Augustinack, J.C., van der Kouwe, A.J., Blackwell, M.L., Salat, D.H., Wiggins, C.J., Frosch, M.P., Wiggins, G.C., Potthast, A., Wald, L.L., Fischl, B.R., 2005. Detection of entorhinal layer II using 7 Tesla [corrected] magnetic resonance imaging. Ann. Neurol. 57, 489–494.
Bakker, A., Kirwan, C.B., Miller, M., Stark, C.E., 2008. Pattern separation in the human hippocampal CA3 and dentate gyrus. Science 319, 1640–1642.
Beckmann, C.F., Jenkinson, M., Smith, S.M., 2003. General multilevel linear modeling for group analysis in FMRI. NeuroImage 20, 1052–1063.
Brown, M.W., Aggleton, J.P., 2001. Recognition memory: what are the roles of the perirhinal cortex and hippocampus? Nat. Rev., Neurosci. 2, 51–61.
Burggren, A.C., Zeineh, M.M., Ekstrom, A.D., Braskie, M.N., Thompson, P.M., Small, G.W., Bookheimer, S.Y., 2008. Reduced cortical thickness in hippocampal subregions among cognitively normal apolipoprotein E e4 carriers. NeuroImage.
Caplan, J.B., Madsen, J.R., Schulze-Bonhage, A., Aschenbrenner-Scheibe, R., Newman, E.L., Kahana, M.J., 2003. Human theta oscillations related to sensorimotor integration and spatial learning. J. Neurosci. 23, 4726–4736.
Cox, R.W., 1996. AFNI: software for analysis and visualization of functional magnetic resonance neuroimages. Comput. Biomed. Res. 29, 162–173.
Duvernoy, H.M., 1998. The Human Hippocampus: Functional Anatomy, Vascularization, and Serial Sections with MRI. Springer, Berlin.
Ekstrom, A., Suthana, N., Behnke, E., B, S.E., Salamon, N., Bookheimer, S., Fried, I., 2008. High-resolution depth electrode localization and imaging in patients with pharmacologically intractable epilepsy. J. Neurosurg. 108, 812–815.
Ekstrom, A.D., Kahana, M.J., Caplan, J.B., Fields, T.A., Isham, E.A., Newman, E.L., Fried, I., 2003. Cellular networks underlying human spatial navigation. Nature 425, 184–188.
Eldridge, L.L., Engel, S.A., Zeineh, M.M., Bookheimer, S.Y., Knowlton, B.J., 2005. A dissociation of encoding and retrieval processes in the human hippocampus. J. Neurosci. 25, 3280–3286.
Engel, S.A., Glover, G.H., Wandell, B.A., 1997. Retinotopic organization in human visual cortex and the spatial precision of functional MRI. Cereb. Cortex 7, 181–192.
Fischl, B., Sereno, M.I., Dale, A.M., 1999. Cortical surface-based analysis. II: inflation, flattening, and a surface-based coordinate system. NeuroImage 9, 195–207.
Friston, K.J., Frith, C.D., Frackowiak, R.S., Turner, R., 1995. Characterizing dynamic brain responses with fMRI: a multivariate approach. NeuroImage 2, 166–172.
Fyhn, M., Molden, S., Witter, M.P., Moser, E.I., Moser, M.B., 2004. Spatial representation in the entorhinal cortex. Science 305, 1258–1264.
Han, X., Jovicich, J., Salat, D., van der Kouwe, A., Quinn, B., Czanner, S., Busa, E., Pacheco, J., Albert, M., Killiany, R., et al., 2006. Reliability of MRI-derived measurements of human cerebral cortical thickness: the effects of field strength, scanner upgrade and manufacturer. NeuroImage 32, 180–194.
Hyde, J.S., Biswal, B.B., Jesmanowicz, A., 2001. High-resolution fMRI using multislice partial k-space GR-EPI with cubic voxels. Magn. Reson. Med. 46 (1), 114–125.
Kirwan, C.B., Jones, C.K., Miller, M.I., Stark, C.E., 2007. High-resolution fMRI investigation of the medial temporal lobe. Hum. Brain Mapp. 28, 959–966.
Lee, I., Yoganarasimha, D., Rao, G., Knierim, J.J., 2004. Comparison of population coherence of place cells in hippocampal subfields CA1 and CA3. Nature 430, 456–459.
Leutgeb, J.K., Leutgeb, S., Moser, M.B., Moser, E.I., 2007. Pattern separation in the dentate gyrus and CA3 of the hippocampus. Science 315, 961–966.
Mathern, G.W., Babb, T.L., Leite, J.P., Pretorius, K., Yeoman, K.M., Kuhlman, P.A., 1996. The pathogenic and progressive features of chronic human hippocampal epilepsy. Epilepsy Res. 26, 151–161.
Miller, M.I., Beg, M.F., Ceritoglu, C., Stark, C., 2005. Increasing the power of functional maps of the medial temporal lobe by using large deformation diffeomorphic metric mapping. Proc. Natl. Acad. Sci. U. S. A. 102, 9685–9690.
Moser, M.B., Moser, E.I., 1998. Functional differentiation in the hippocampus. Hippocampus 8, 608–619.
Oliver, P., Shapiro, G., Tannenbaum, A., 1997. Invariant geometric evolutions of surfaces and volumetric smoothing. SIAM J. Appl. Math. 57, 176–194.
Sharp, P.E., 2006. Subicular place cells generate the same "map" for different environments: comparison with hippocampal cells. Behav. Brain Res. 174, 206–214.
Sharp, P.E., Green, C., 1994. Spatial correlates of firing patterns of single cells in the subiculum of the freely moving rat. J. Neurosci. 14, 2339–2356.
Shipman, S.L., Astur, R.S., 2008. Factors affecting the hippocampal BOLD response during spatial memory. Behav. Brain Res. 187, 433–441.
Stark, C.E., Okado, Y., 2003. Making memories without trying: medial temporal lobe activity associated with incidental memory formation during recognition. J. Neurosci. 23, 6748–6753.
Stark, C.E., Squire, L.R., 2001. When zero is not zero: the problem of ambiguous baseline conditions in fMRI. Proc. Natl. Acad. Sci. U. S. A. 98, 12760–12766.
Teo, P.C., Sapiro, G., Wandell, B.A., 1997. Creating connected representations of cortical gray matter for functional MRI visualization. IEEE Trans. Med. Imaging 16, 852–863.
Thompson, P.M., Woods, R.P., Mega, M.S., Toga, A.W., 2000. Mathematical/computational challenges in creating deformable and probabilistic atlases of the human brain. Hum. Brain Mapp. 9, 81–92.
Wilson, M.A., McNaughton, B.L., 1993. Dynamics of the hippocampal ensemble code for space. Science 261, 1055–1058.
Woolrich, M.W., Ripley, B.D., Brady, M., Smith, S.M., 2001. Temporal autocorrelation in univariate linear modeling of FMRI data. NeuroImage 14, 1370–1386.
Zeineh, M.M., Engel, S.A., Bookheimer, S.Y., 2000. Application of cortical unfolding techniques to functional MRI of the human hippocampal region. NeuroImage 11, 668–683.
Zeineh, M.M., Engel, S.A., Thompson, P.M., Bookheimer, S.Y., 2001. Unfolding the human hippocampus with high resolution structural and functional MRI. Anat. Rec. 265, 111–120.
Zeineh, M.M., Engel, S.A., Thompson, P.M., Bookheimer, S.Y., 2003. Dynamics of the hippocampus during encoding and retrieval of face-name pairs. Science 299, 577–580.